LAWRENCE
LIVERMORE
NATIONAL
LABORATORY

UCRL-JRNL-218514

# Accurate and stable finite difference approximations of the elastodynamic equations in second order formulation

Stefan Nilsson, N. Anders Petersson, Björn Sjögreen, Heinz-Otto Kreiss

January 30, 2006

Journal of computational physics

**Disclaimer**

This document was prepared as an account of work sponsored by an agency of the United States Government. Neither the United States Government nor the University of California nor any of their employees, makes any warranty, express or implied, or assumes any legal liability or responsibility for the accuracy, completeness, or usefulness of any information, apparatus, product, or process disclosed, or represents that its use would not infringe privately owned rights. Reference herein to any specific commercial product, process, or service by trade name, trademark, manufacturer, or otherwise, does not necessarily constitute or imply its endorsement, recommendation, or favoring by the United States Government or the University of California. The views and opinions of authors expressed herein do not necessarily state or reflect those of the United States Government or the University of California, and shall not be used for advertising or product endorsement purposes.

# Accurate and stable finite difference approximations of the elastodynamic equations in second order formulation*

Stefan Nilsson†, N. Anders Petersson†, Björn Sjögreen†, and Heinz-Otto Kreiss‡

January 30, 2006

**Abstract**

We present a finite difference method for computing elastic waves. It is based on writing the elastodynamic equations in second order formulation. The method is second order accurate in space and time, and conserves a discrete energy norm. Therefore it is stable for rapidly changing properties of the elastic material. In many applications, e.g. seismology, the source terms are in the form of Dirac distributions in space and the solutions contain local singularities. We describe some observations on the convergence properties and modeling of the source terms. We have also successfully carried out extensive verifications on standard test cases with known solutions. Furthermore, example calculations from seismology performed with a parallel code implementing the method are given.

## 1 Introduction

This paper represents the first part of an effort to construct a fast, robust, and accurate computational method for elastodynamic problems. The basic discretization method is finite differences and we have used seismic waves as a first application, allowing us to concentrate on simple geometries such as half spaces. The new method is designed to preserve a discrete energy norm and is therefore stable for all problems were the material properties are within the limits imposed by physics.

Wave propagation in elastic media has a wide range of application areas. Some examples are seismology, non-destructive evaluation and medical imaging. The underlying mathematical theory of elastodynamics has produced analytical solutions for a number of basic problems since its inception in 1820. However, due to either complicated geometries (in engineering) or complex material properties (in medicine and earth sciences), the need for numerical approximations is great.

The importance of application areas such as seismology led to early use of computers in elastodynamics [20]. As computers have increased in speed and memory they have been applied to larger and more advanced problems, a trend that continues today [9]. Finite difference approximations of the elastodynamic equations have also been around for a long time (see [1] for examples). Early methods were based on standard central difference approximations and were initially very successful. However, they suffered from instabilities originating from the discretized boundary conditions whenever the material properties were outside certain ranges. A description of this difficulty can be found in [10] and [11] where a remedy, valid for materials with properties not varying in the direction normal to the boundary, is also suggested. A more general but also more computationally expensive solution is suggested in [22].

*This work was performed under the auspices of the U.S. Department of Energy by University of California Lawrence Livermore National Laboratory under contract No. W-7405-Eng-48.

†Center for Applied Scientific Computing, Lawrence Livermore National Laboratory, Livermore, CA 94551, USA ({nilsson2,andersp,sjogreen2}@llnl.gov)

‡Träskö-Storö Institute of Mathematics, Stockholm, Sweden

The properties of the non-linear elastic equations are still not fully understood [2], but the linear approximations used in this paper are considered satisfactory for many applications.

Assuming small, adiabatic strains, waves propagating in solids are described by the elastic wave equation for the displacement vector $\mathbf{u}$

$$\rho \mathbf{u}_{tt} = \nabla \cdot \mathfrak{T} + \rho \mathbf{f}, \tag{1}$$

where $\rho$ represents density, the vector $\mathbf{f}$ is a source term and the stress tensor $\mathfrak{T}$ is given by Hooke's law as the contraction over two indices of the fourth-order elastic moduli tensor $\mathbf{C}$ and the second-order strain tensor $\mathfrak{E} = 1/2(\nabla \mathbf{u} + (\nabla \mathbf{u})^T)$,

$$\mathfrak{T} = \mathbf{C} : \mathfrak{E}.$$

Continuity of the stress field implies that for a boundary with normal vector $\hat{\mathbf{n}}$, we have

$$\mathfrak{T}\hat{\mathbf{n}} = \mathbf{g}, \tag{2}$$

where $\mathbf{g}$ represents applied stress. If $\mathbf{g} = \mathbf{0}$, we obtain what is called the stress free boundary condition.

Equation (1) with boundary condition (2) fulfills the standard continuum mechanical energy estimate for a domain $\Omega$ with boundary $\partial\Omega$:

$$\frac{d}{dt} \int_\Omega \frac{1}{2} \left( \rho \left| \mathbf{u}_t \right|^2 + \mathfrak{T} : \mathfrak{E} \right) \, dV = \int_{\partial\Omega} \mathbf{g} \cdot \mathbf{u}_t \, dS + \int_\Omega \rho \left( \mathbf{f} \cdot \mathbf{u}_t \right) \, dV. \tag{3}$$

Isotropic, non-homogeneous materials can be completely described using only the three parameters $\rho = \rho(\mathbf{x})$, $\mu = \mu(\mathbf{x})$, $\lambda = \lambda(\mathbf{x})$, where the last two are called the Lamé parameters and completely determines $\mathbf{C}$ for this case. Using these three parameters, (1) becomes

$$\rho \frac{\partial^2 \mathbf{u}}{\partial t^2} = \nabla(\lambda \nabla \cdot \mathbf{u}) + \nabla \cdot (\mu \nabla \mathbf{u}) + \nabla \cdot (\mu (\nabla \mathbf{u})^T) + \rho \mathbf{f}, \tag{4}$$

and the stress free boundary condition becomes

$$\lambda (\nabla \cdot \mathbf{u}) \hat{\mathbf{n}} + (\mu \nabla \mathbf{u} + \mu (\nabla \mathbf{u})^T)) \cdot \hat{\mathbf{n}} = \mathbf{0}. \tag{5}$$

The system described by (4) admits wave solutions with two characteristic speeds, $c_p = \sqrt{(2\mu + \lambda)/\rho}$ for longitudinal waves and $c_s = \sqrt{\mu/\rho}$ for transverse waves. The focus of this paper is on solving (4) in a half-space $z \geq 0$, subject to (5) on the $z = 0$ boundary.

For the isotropic case the integral on the left hand side of (3), which is the sum of the kinetic energy and the potential elastic energy becomes

$$\int_\Omega \frac{1}{2} \rho \left| \mathbf{u}_t \right|^2 + \mu \, \mathrm{Tr} \, \mathfrak{E}^2 + \frac{1}{2} \lambda (\mathrm{Tr} \, \mathfrak{E})^2 \, dV, \tag{6}$$

where Tr is the trace operator.

For constant values of $\mu > 0$ and $\lambda > 0$, (4) together with the stress free boundary condition (5) is also known to be weakly well-posed in $L^2$ [4].

The problems encountered by the early finite difference approximations of (4) when the ratio of $c_p$ over $c_s$ became too large led to alternative formulations where the elastic wave equation was rewritten as a first order system. Computer codes were then based on discretizations of these first order formulations on staggered grids [18]. Most later efforts for finite difference methods have worked with first order systems. In later years more expensive methods such as spectral element [12] and the pseudo-spectral method have also gained in popularity.

Our new method solves (4) directly in second order formulation. The reason for choosing the second order formulation is that we in future work want to include embedded boundaries to allow the inclusion of

topography and other geometric features, building on the technique developed for the second order scalar wave equation in [13] and [16]. Furthermore we can prove that our method conserves a discrete energy for a domain with either prescribed stress and/or prescribed displacements on the boundary, regardless of material properties as long as $\lambda > 0$ and $\mu > 0$ holds true at all grid points.

In Section 2 we give a extensive description of our new finite difference method that avoids the stability problems that have plagued earlier discretizations of the elastodynamic equations in second order formulation. The accuracy of the new method is illustrated with computational results. The problem of computing elastic waves in truncated domains necessitates the use of non-reflecting boundary conditions. A brief description of a simple variant of such a condition is found in Section 3. Seismic events are often modeled using singular source terms and these are analyzed in Section 4. In Section 5 we illustrate the viability of our approach with examples from real world applications. Finally in Section 6 we discuss the results and give some plans for possible extensions of our method.

# 2 Discretizing the elastic wave equation

## 2.1 Preliminary assumptions

Let the displacement vector $\mathbf{u} = \mathbf{u}(\mathbf{x}, t)$ have Cartesian components $\mathbf{u} = (u, v, w)^T$, where $\mathbf{x} = (x, y, z)^T$ is the location and $t$ is time. To simplify the presentation, we take $\mathbf{f} = \mathbf{0}$ and $\mathbf{g} = \mathbf{0}$ throughout this section. In component form, the governing equations are

$$\rho u_{tt} = \frac{\partial}{\partial x}\left((2\mu+\lambda)u_x + \lambda v_y + \lambda w_z\right) + \frac{\partial}{\partial y}\left(\mu v_x + \mu u_y\right) + \frac{\partial}{\partial z}\left(\mu u_z + \mu w_x\right), \tag{7}$$

$$\rho v_{tt} = \frac{\partial}{\partial x}\left(\mu v_x + \mu u_y\right) + \frac{\partial}{\partial y}\left((2\mu+\lambda)v_y + \lambda u_x + \lambda w_z\right) + \frac{\partial}{\partial z}\left(\mu v_z + \mu w_y\right), \tag{8}$$

$$\rho w_{tt} = \frac{\partial}{\partial x}\left(\mu u_z + \mu w_x\right) + \frac{\partial}{\partial y}\left(\mu v_z + \mu w_y\right) + \frac{\partial}{\partial z}\left((2\mu+\lambda)w_z + \lambda u_x + \lambda v_y\right), \tag{9}$$

in the domain $0 \le x \le a$, $0 \le y \le b$, $0 \le z \le c$, $t \ge 0$, subject to initial conditions

$$u(\mathbf{x}, 0) = U_0(\mathbf{x}), \quad v(\mathbf{x}, 0) = V_0(\mathbf{x}), \quad w(\mathbf{x}, 0) = W_0(\mathbf{x}), \tag{10}$$

$$u_t(\mathbf{x}, 0) = U_1(\mathbf{x}), \quad v_t(\mathbf{x}, 0) = V_1(\mathbf{x}), \quad w_t(\mathbf{x}, 0) = W_1(\mathbf{x}). \tag{11}$$

We impose a stress-free boundary condition at $z = 0$. In component form

$$\mu u_z + \mu w_x = 0, \tag{12}$$

$$\mu v_z + \mu w_y = 0, \quad z = 0,\ 0 \le x \le a,\ 0 \le y \le b,\ t \ge 0, \tag{13}$$

$$(2\mu+\lambda)w_z + \lambda u_x + \lambda v_y = 0. \tag{14}$$

For the purpose of discussing energy conservation, we impose homogeneous Dirichlet conditions at $z = c$, and periodic boundary conditions in the $x$ and $y$-directions,

$$\mathbf{u}(x, y, c) = 0, \qquad 0 \le x \le a,\ 0 \le y \le b,\ t \ge 0, \tag{15}$$

$$\mathbf{u}(0, y, z) = \mathbf{u}(a, y, z), \quad \mathbf{u}_x(0, y, z) = \mathbf{u}_x(a, y, z), \quad 0 \le y \le b,\ 0 \le z \le c,\ t \ge 0, \tag{16}$$

$$\mathbf{u}(x, 0, z) = \mathbf{u}(x, b, z), \quad \mathbf{u}_y(x, 0, z) = \mathbf{u}_y(x, b, z), \quad 0 \le x \le a,\ 0 \le z \le c,\ t \ge 0. \tag{17}$$

Note that energy conservation can also be obtained when the periodic boundary conditions are replaced by homogeneous Dirichlet conditions for the displacement.

## 2.2 Spatial discretization

We introduce a grid with grid points $x_i = (i-1)h$, $y_j = (j-1)h$, $z_k = (k-1)h$ where $h > 0$ is the grid size and $x_{N_x} = a$, $y_{N_y} = b$, $z_{N_z} = c$. Time is discretized with step size $\delta_t > 0$ on a grid $t_n = n\delta_t$, $n = 0, 1, \ldots$, and we denote a grid function by $u^n_{i,j,k} = u(x_i, y_j, z_k, t_n)$. The superscript for time will be suppressed when the meaning is obvious. We use the usual definitions of divided difference operators,

$$D^x_+ v_{i,j,k} = \frac{1}{h}(v_{i+1,j,k} - v_{i,j,k}), \quad D^x_- v_{i,j,k} = D^x_+ v_{i-1,j,k}, \quad D^x_0 = \frac{1}{2}\left(D^x_+ + D^x_-\right),$$

and corresponding expressions in the $y$ and $z$-directions. We also define

$$\widetilde{D^z_0} v_{i,j,k} = \begin{cases} D^z_+ v_{i,j,1}, & k = 1, \\ D^z_0 v_{i,j,k}, & k \geq 2, \end{cases}$$

and the shift operators

$$\begin{aligned} E^x_{1/2}(\gamma_{i,j,k}) &= \gamma_{i+1/2,j,k} := \frac{\gamma_{i+1,j,k} + \gamma_{i,j,k}}{2}, \\ E^y_{1/2}(\gamma_{i,j,k}) &= \gamma_{i,j+1/2,k} := \frac{\gamma_{i,j+1,k} + \gamma_{i,j,k}}{2}, \\ E^z_{1/2}(\gamma_{i,j,k}) &= \gamma_{i,j,k+1/2} := \frac{\gamma_{i,j,k+1} + \gamma_{i,j,k}}{2}. \end{aligned}$$

We form the spatially discrete equations at the grid points $1 \leq i \leq N_x - 1$, $1 \leq j \leq N_y - 1$, $1 \leq k \leq N_z - 1$. Grid point indices are suppressed to improve readability.

$$\begin{aligned} \rho \frac{d^2 u}{dt^2} &= D^x_- \left(E^x_{1/2}(2\mu + \lambda) D^x_+ u\right) + D^y_- \left(E^y_{1/2}(\mu) D^y_+ u\right) + D^z_- \left(E^z_{1/2}(\mu) D^z_+ u\right) \\ &\quad + D^x_0 \left(\lambda D^y_0 v + \lambda \widetilde{D^z_0} w\right) + D^y_0 \left(\mu D^x_0 v\right) + \widetilde{D^z_0} \left(\mu D^x_0 w\right) =: L^{(u)}(u, v, w), \end{aligned} \tag{18}$$

$$\begin{aligned} \rho \frac{d^2 v}{dt^2} &= D^x_- \left(E^x_{1/2}(\mu) D^x_+ v\right) + D^y_- \left(E^y_{1/2}(2\mu + \lambda) D^y_+ v\right) + D^z_- \left(E^z_{1/2}(\mu) D^z_+ v\right) \\ &\quad + D^x_0 \left(\mu D^y_0 u\right) + D^y_0 \left(\lambda D^x_0 u + \lambda \widetilde{D^z_0} w\right) + \widetilde{D^z_0} \left(\mu D^y_0 w\right) =: L^{(v)}(u, v, w), \end{aligned} \tag{19}$$

$$\begin{aligned} \rho \frac{d^2 w}{dt^2} &= D^x_- \left(E^x_{1/2}(\mu) D^x_+ w\right) + D^y_- \left(E^y_{1/2}(\mu) D^y_+ w\right) + D^z_- \left(E^z_{1/2}(2\mu + \lambda) D^z_+ w\right) \\ &\quad + D^x_0 \left(\mu \widetilde{D^z_0} u\right) + D^y_0 \left(\mu \widetilde{D^z_0} v\right) + \widetilde{D^z_0} \left(\lambda D^x_0 u + \lambda D^y_0 v\right) =: L^{(w)}(u, v, w). \end{aligned} \tag{20}$$

**Note:** The discrete solution will be second order accurate in space, even though $\widetilde{D^z_0}$ reduces to a one-sided divided difference operator on the boundary, see Lemma 4 below.

The free surface boundary conditions (12)-(14) are discretized by

$$\frac{1}{2}\left(\mu_{i,j,3/2} D^z_+ u_{i,j,1} + \mu_{i,j,1/2} D^z_+ u_{i,j,0}\right) + \mu_{i,j,1} D^x_0 w_{i,j,1} = 0, \tag{21}$$

$$\frac{1}{2}\left(\mu_{i,j,3/2} D^z_+ v_{i,j,1} + \mu_{i,j,1/2} D^z_+ v_{i,j,0}\right) + \mu_{i,j,1} D^y_0 w_{i,j,1} = 0, \tag{22}$$

$$\frac{1}{2}\left((2\mu + \lambda)_{i,j,3/2} D^z_+ w_{i,j,1} + (2\mu + \lambda)_{i,j,1/2} D^z_+ w_{i,j,0}\right) + \lambda_{i,j,1}\left(D^x_0 u_{i,j,1} + D^y_0 v_{i,j,1}\right) = 0, \tag{23}$$

for $2 \leq i \leq N_x - 1$, $2 \leq j \leq N_y - 1$. The Dirichlet boundary condition (15) is discretized by

$$\mathbf{u}_{i,j,N_z} = 0, \tag{24}$$

for $1 \le i \le N_x,\ 1 \le j \le N_y$. The discrete counterpart of the periodic boundary conditions (16) and (17) are

$$\mathbf{u}_{N_x,j,k} = \mathbf{u}_{1,j,k}, \quad \mathbf{u}_{0,j,k} = \mathbf{u}_{N_x-1,j,k}, \tag{25}$$

$$\mathbf{u}_{i,N_y,k} = \mathbf{u}_{i,1,k}, \quad \mathbf{u}_{i,0,k} = \mathbf{u}_{i,N_y-1,k}, \tag{26}$$

for $1 \le i \le N_x,\ 1 \le j \le N_y,\ 1 \le k \le N_z$.

We proceed by showing that the above scheme satisfies an energy estimate. We first define a weighted scalar product and norm:

$$(w,v)_h = h^2 \sum_{i=1}^{N_x-1} \sum_{j=1}^{N_y-1} \left( \frac{h}{2} w_{i,j,1} v_{i,j,1} + h \sum_{k=2}^{N_z-1} w_{i,j,k} v_{i,j,k} \right), \quad \|v\|_h^2 = (v,v)_h.$$

Our proof of stability of the scheme relies on the spatial discretization being self-adjoint and negative definite (elliptic). The self-adjoint property is expressed in

**Lemma 1** *For all real-valued grid functions $(u^0, v^0, w^0)$, $(u^1, v^1, w^1)$ which satisfy the discrete boundary conditions (21)-(23), (24), and the periodicity conditions (25)-(26), the spatial operator $(L^{(u)}, L^{(v)}, L^{(w)})$ is self-adjoint, i.e.,*

$$\begin{aligned} \left(u^0, L^{(u)}(u^1,v^1,w^1)\right)_h + \left(v^0, L^{(v)}(u^1,v^1,w^1)\right)_h + \left(w^0, L^{(w)}(u^1,v^1,w^1)\right)_h = \\ \left(u^1, L^{(u)}(u^0,v^0,w^0)\right)_h + \left(v^1, L^{(v)}(u^0,v^0,w^0)\right)_h + \left(w^1, L^{(w)}(u^0,v^0,w^0)\right)_h. \end{aligned} \tag{27}$$

**Proof:** See appendix A. □

From the self-adjoint property it follows that there exists a conserved quantity:

**Lemma 2** *All real-valued solutions $(u,v,w)$ of the semi-discrete scheme (18)-(20) subject to the boundary conditions (21)-(23), (24), and the periodicity conditions (25)-(26), satisfy*

$$\|\rho^{1/2} u_t\|_h^2 + \|\rho^{1/2} v_t\|_h^2 + \|\rho^{1/2} w_t\|_h^2 - (u, L^{(u)}(u,v,w))_h - (v, L^{(v)}(u,v,w))_h - (w, L^{(w)}(u,v,w))_h = C, \tag{28}$$

*where $C$ is a constant which depends on the initial data and*

$$\begin{aligned} \left(u, L^{(u)}(u,v,w)\right)_h = &- \left(D_+^x u, E_{1/2}^x (2\mu+\lambda) D_+^x u\right)_h - \left(D_+^y u, E_{1/2}^y (\mu) D_+^y u\right)_h \\ &- \left(D_+^z u, E_{1/2}^z (\mu) D_+^z u\right)_h - \left(D_0^x u, \lambda D_0^y v + \lambda \widetilde{D}_0^z w\right)_h - (D_0^y u, \mu D_0^x v)_h \\ &- \left(\widetilde{D}_0^z u, \mu D_0^x w\right)_h - \frac{h^3}{2} \sum_{i,j} \mu_{i,j,3/2} (D_+^z u_{i,j,1})^2, \end{aligned} \tag{29}$$

$$\begin{aligned} \left(v, L^{(v)}(u,v,w)\right)_h = &- \left(D_+^x v, E_{1/2}^x (\mu) D_+^x v\right)_h - \left(D_+^y v, E_{1/2}^y (2\mu+\lambda) D_+^y v\right)_h \\ &- \left(D_+^z v, E_{1/2}^z (\mu) D_+^z v\right)_h - (D_0^x v, \mu D_0^y u)_h - \left(D_0^y v, \lambda D_0^x u + \lambda \widetilde{D}_0^z w\right)_h \\ &- \left(\widetilde{D}_0^z v, \mu D_0^y w\right)_h - \frac{h^3}{2} \sum_{i,j} \mu_{i,j,3/2} (D_+^z v_{i,j,1})^2, \end{aligned} \tag{30}$$

$$\left(w, L^{(w)}(u,v,w)\right)_h = -\left(D_+^x w, E_{1/2}^x(\mu) D_+^x w\right)_h - \left(D_+^y w, E_{1/2}^y(\mu) D_+^y w\right)_h$$
$$- \left(D_+^z w, E_{1/2}^z(2\mu+\lambda) D_+^z w\right)_h - \left(D_0^x w, \mu \widetilde{D_0^z} u\right)_h - \left(D_0^y w, \mu \widetilde{D_0^z} v\right)_h$$
$$- \left(\widetilde{D_0^z} w, \lambda D_0^x u + \lambda D_0^y v\right)_h - \frac{h^3}{2} \sum_{i,j} (2\mu_{i,j,3/2} + \lambda_{i,j,3/2})(D_+^z w_{i,j,1})^2. \quad (31)$$

**Proof:** Lemma 1 gives

$$\frac{1}{2}\frac{d}{dt}\left(\|\rho^{1/2} u_t\|_h^2 + \|\rho^{1/2} v_t\|_h^2 + \|\rho^{1/2} w_t\|_h^2\right) =$$
$$(u_t, L^{(u)}(u,v,w))_h + (v_t, L^{(v)}(u,v,w))_h + (w_t, L^{(w)}(u,v,w))_h =$$
$$\frac{1}{2}\left((u_t, L^{(u)}(u,v,w))_h + (v_t, L^{(v)}(u,v,w))_h + (w_t, L^{(w)}(u,v,w))_h\right)$$
$$+ \frac{1}{2}\left((u, L^{(u)}(u_t,v_t,w_t))_h + (v, L^{(v)}(u_t,v_t,w_t))_h + (w, L^{(w)}(u_t,v_t,w_t))_h\right) =$$
$$\frac{1}{2}\frac{d}{dt}\left((u, L^{(u)}(u,v,w))_h + (v, L^{(v)}(u,v,w))_h + (w, L^{(w)}(u,v,w))_h\right).$$

Integrating the above relation in time starting at $t = 0$ gives (28) and shows that the constant $C$ depends on the initial data. Equations (29), (30), and (31) follow from the proof of Lemma 1 by setting $(u^0, v^0, w^0) = (u^1, v^1, w^1) = (u, v, w)$ in (54), (56), and (57). □

To prove that the scheme is stable, we need to show that the conserved quantity in (28) is a norm, that is, we need to show that the spatial operator is negative definite. In particular, we need to show that the sum of the mixed terms in (29), (30), and (31), (such as $\left(D_0^x w, \mu \widetilde{D_0^z} u\right)_h$), is dominated by the sum of the strictly positive terms (such as $\left(D_+^x w, E_{1/2}^x(\mu) D_+^x w\right)_h$ when $\mu > 0$). This is straight forward in the corresponding continuous case and leads to the well known formula for the elastic energy. What makes the discrete case more challenging is that all derivatives in the strictly positive terms are discretized by compact operators (such as $D_+^x$), while they are discretized by centered differences (such as $D_0^x$) in all mixed terms. While numerous numerical experiments indicate that the conserved quantity (28) always is positive for positive $\mu$ and $\lambda$, we only prove this property in the fully periodic case, i.e., when the free surface boundary conditions (21)-(23) and the Dirichlet condition (24) are replaced by

$$\mathbf{u}_{i,j,N_z} = \mathbf{u}_{i,j,1}, \quad \mathbf{u}_{i,j,0} = \mathbf{u}_{i,j,N_z-1}, \quad 1 \le i \le N_x,\ 1 \le j \le N_y. \quad (32)$$

To match the periodic boundary conditions, we define modified spatial operators $\widetilde{L}^{(u)}$, $\widetilde{L}^{(v)}$, and $\widetilde{L}^{(w)}$ by replacing $\widetilde{D_0^z}$ by $D_0^z$ in (18)-(20). Furthermore, we also need a basic scalar product and norm for the fully periodic case,

$$(w,v)_2 = h^3 \sum_{i=1}^{N_x-1} \sum_{i=1}^{N_y-1} \sum_{k=1}^{N_z-1} w_{i,j,k} v_{i,j,k}, \quad \|w\|_2^2 = (w,w)_2.$$

We have

**Lemma 3** *For all real valued grid functions $(u,v,w)$ which satisfy the periodic boundary conditions (25)-(26), (32) the operator $\left(\widetilde{L}^{(u)}, \widetilde{L}^{(v)}, \widetilde{L}^{(w)}\right)$ is negative definite when $\mu > 0$ and $\lambda > 0$; it is semi-definite when $\mu = 0$ and $\lambda > 0$, it is indefinite when $\mu < 0$ and $\lambda > 0$, and it is positive definite when $\mu < 0$ and*

$\lambda \leq 0$. *In particular,*

$$
\begin{aligned}
-\left(u,\widetilde{L}^{(u)}(u,v,w)\right)_2 - \left(v,\widetilde{L}^{(v)}(u,v,w)\right)_2 - \left(w,\widetilde{L}^{(w)}(u,v,w)\right)_2 = \\
2\left(D_+^x u, E_{1/2}^x(\mu) D_+^x u\right)_2 + 2\left(D_+^y v, E_{1/2}^y(\mu) D_+^y v\right)_2 + 2\left(D_+^z w, E_{1/2}^z(\mu) D_+^z w\right)_2 \\
+ (D_0^y u + D_0^x v, \mu(D_0^y u + D_0^x v))_2 \\
+ (D_0^z u + D_0^x w, \mu(D_0^z u + D_0^x w))_2 \\
+ (D_0^z v + D_0^y w, \mu(D_0^z v + D_0^y w))_2 \\
+ (D_0^x u + D_0^y v + D_0^z w, \lambda(D_0^x u + D_0^y v + D_0^z w))_2 + h^2 R/4, \quad (33)
\end{aligned}
$$

*where the remainder term is*

$$
\begin{aligned}
R = \left(D_+^x D_-^x u, \lambda D_+^x D_-^x u\right)_2 + \left(D_+^y D_-^y u, \mu D_+^y D_-^y u\right)_2 + \left(D_+^z D_-^z u, \mu D_+^z D_-^z u\right)_2 \\
+ \left(D_+^x D_-^x v, \mu D_+^x D_-^x v\right)_2 + \left(D_+^y D_-^y v, \lambda D_+^y D_-^y v\right)_2 + \left(D_+^z D_-^z v, \mu D_+^z D_-^z v\right)_2 \\
+ \left(D_+^x D_-^x w, \mu D_+^x D_-^x w\right)_2 + \left(D_+^y D_-^y w, \mu D_+^y D_-^y w\right)_2 + \left(D_+^z D_-^z w, \lambda D_+^z D_-^z w\right)_2 . \quad (34)
\end{aligned}
$$

**Proof:** Equations (33) and (34) are derived in appendix B. When $\mu > 0$ and $\lambda > 0$, all terms are positive and the operator $\left(\widetilde{L}^{(u)}, \widetilde{L}^{(v)}, \widetilde{L}^{(w)}\right)$ is negative definite. When $\mu = 0$ and $\lambda > 0$, the operator has a null-space consisting of grid functions with zero discrete divergence. When $\mu < 0$, all terms containing $\mu$ are negative. If also $\lambda < 0$, all terms become negative and the operator becomes positive definite. □

The accuracy of the solution is governed by

**Lemma 4** *The solution of the semi-discrete scheme (18)-(20) subject to the boundary conditions (21)-(23) and (24) is a second order accurate approximation of the solution of the continuous equation (7)-(9) subject to the boundary conditions (12)-(14) and (15).*

**Proof:** See appendix C. □

## 2.3 Fully discrete equations

We discretize (18)-(20) in time according to

$$\rho\left(\frac{u^{n+1} - 2u^n + u^{n-1}}{\delta_t^2}\right) = L^{(u)}(u^n, v^n, w^w), \quad (35)$$

$$\rho\left(\frac{v^{n+1} - 2v^n + v^{n-1}}{\delta_t^2}\right) = L^{(v)}(u^n, v^n, w^w), \quad (36)$$

$$\rho\left(\frac{w^{n+1} - 2w^n + w^{n-1}}{\delta_t^2}\right) = L^{(w)}(u^n, v^n, w^w). \quad (37)$$

For simplicity, we introduce the weighted norm

$$(w,v)_\rho = h^2 \sum_{i=1}^{N_x-1} \sum_{j=1}^{N_y-1} \left(\frac{h}{2}\rho_{i,j,1} w_{i,j,1} v_{i,j,1} + h \sum_{k=2}^{N_z-1} \rho_{i,j,k} w_{i,j,k} v_{i,j,k}\right), \quad \|v\|_\rho^2 = (v,v)_\rho .$$

Trivial calculations show

$$\left(w, \rho^{-1} v\right)_\rho = (w,v)_h . \quad (38)$$

To show that the fully discrete scheme is energy conserving, we consider the quantity

$$\begin{aligned} C_e(t_{n+1}) &= \left\|D_+^t u^n\right\|_\rho^2 + \left\|D_+^t v^n\right\|_\rho^2 + \left\|D_+^t w^n\right\|_\rho^2 - \left(u^{n+1}, \rho^{-1} L^{(u)}(u^n, v^n, w^n)\right)_\rho \\ &\quad - \left(v^{n+1}, \rho^{-1} L^{(v)}(u^n, v^n, w^n)\right)_\rho - \left(w^{n+1}, \rho^{-1} L^{(w)}(u^n, v^n, w^n)\right)_\rho \\ &= \left\|D_+^t u^n\right\|_\rho^2 + \left\|D_+^t v^n\right\|_\rho^2 + \left\|D_+^t w^n\right\|_\rho^2 \\ &\quad - \left(u^{n+1}, D_+^t D_-^t u^n\right)_\rho - \left(v^{n+1}, D_+^t D_-^t v^n\right)_\rho - \left(w^{n+1}, D_+^t D_-^t w^n\right)_\rho \end{aligned}$$

It can be shown that $C_e > 0$ when the time step satisfies $\delta_t \leq C_{CFL} h$, where $C_{CFL}$ is the Courant number that guarantees stability of the explicit scheme (35)-(37), see [15]. Furthermore,

$$\begin{aligned} \delta_t^2 C_e(t_{n+1}) = \|u^{n+1}\|_\rho^2 + \|u^n\|_\rho^2 - \left(u^{n+1}, 2u^n + \delta_t^2 \rho^{-1} L^{(u)}(u^n, v^n, w^n)\right)_\rho + \\ \|v^{n+1}\|_\rho^2 + \|v^n\|_\rho^2 - \left(v^{n+1}, 2v^n + \delta_t^2 \rho^{-1} L^{(v)}(u^n, v^n, w^n)\right)_\rho + \\ \|w^{n+1}\|_\rho^2 + \|w^n\|_\rho^2 - \left(w^{n+1}, 2w^n + \delta_t^2 \rho^{-1} L^{(w)}(u^n, v^n, w^n)\right)_\rho . \quad (39) \end{aligned}$$

We have,

$$u^{n+1} + u^{n-1} = 2u^n + \delta_t^2 \rho^{-1} L^{(u)}(u^n, v^n, w^n),$$

and corresponding expressions for $v$ and $w$. Hence,

$$\begin{aligned} \delta_t^2 C_e(t_{n+1}) &= \|u^{n+1}\|_\rho^2 + \|u^n\|_\rho^2 - \left(u^{n+1}, u^{n+1} + u^{n-1}\right)_\rho + \|v^{n+1}\|_\rho^2 + \|v^n\|_\rho^2 - \\ &\quad \left(v^{n+1}, v^{n+1} + v^{n-1}\right)_\rho + \|w^{n+1}\|_\rho^2 + \|w^n\|_\rho^2 - \left(w^{n+1}, w^{n+1} + w^{n-1}\right)_\rho \\ &= \|u^n\|_\rho^2 + \|u^{n-1}\|_\rho^2 - \left(u^{n-1}, 2u^n + \delta_t^2 \rho^{-1} L^{(u)}(u^n, v^n, w^n)\right)_\rho + \\ &\quad \|v^n\|_\rho^2 + \|v^{n-1}\|_\rho^2 - \left(v^{n-1}, 2v^n + \delta_t^2 \rho^{-1} L^{(v)}(u^n, v^n, w^n)\right)_\rho + \\ &\quad \|w^n\|_\rho^2 + \|w^{n-1}\|_\rho^2 - \left(w^{n-1}, 2w^n + \delta_t^2 \rho^{-1} L^{(w)}(u^n, v^n, w^n)\right)_\rho . \end{aligned}$$

The relation (38) gives

$$\left(u^{n-1}, \delta_t^2 \rho^{-1} L^{(u)}(u^n, v^n, w^n)\right)_\rho = \left(u^{n-1}, \delta_t^2 L^{(u)}(u^n, v^n, w^n)\right)_h ,$$

so Lemma 1 gives

$$\begin{aligned} \left(u^{n-1}, \delta_t^2 \rho^{-1} L^{(u)}(u^n, v^n, w^n)\right)_\rho + \left(v^{n-1}, \delta_t^2 \rho^{-1} L^{(v)}(u^n, v^n, w^n)\right)_\rho + \\ \left(w^{n-1}, \delta_t^2 \rho^{-1} L^{(w)}(u^n, v^n, w^n)\right)_\rho = \\ \left(u^n, \delta_t^2 \rho^{-1} L^{(u)}(u^{n-1}, v^{n-1}, w^{n-1})\right)_\rho + \left(v^n, \delta_t^2 \rho^{-1} L^{(v)}(u^{n-1}, v^{n-1}, w^{n-1})\right)_\rho + \\ \left(w^n, \delta_t^2 \rho^{-1} L^{(w)}(u^{n-1}, v^{n-1}, w^{n-1})\right)_\rho . \quad (40) \end{aligned}$$

We conclude that

$$C_e(t_{n+1}) = C_e(t_n),$$

that is, $C_e(t_n)$ is a conserved quantity for the fully discrete scheme. It is straight forward to show that $C_e$ is a second order accurate approximation of the continuous elastic energy (6).

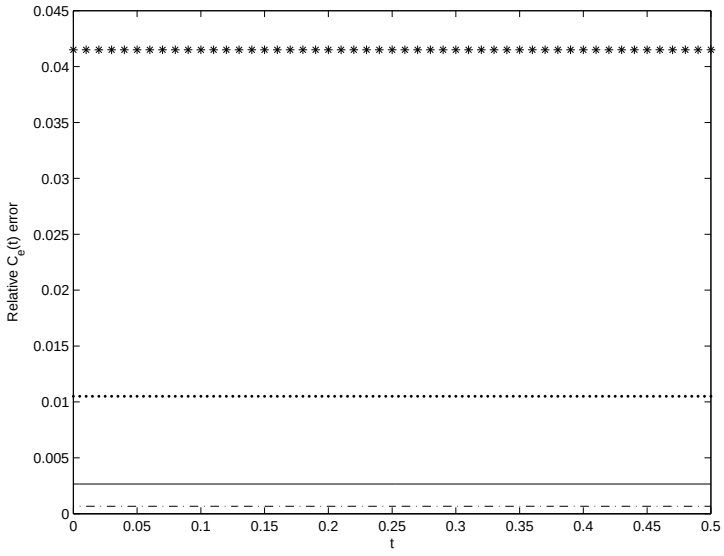


Figure 1: Relative error in discrete energy $C_e(t)$ as compared to the continuous energy (6) for different grid sizes. The energy is conserved to within round off errors for all cases. As can be seen the discrete energy converges towards the continuous value with second order in $h$, as expected. $h = 0.04\,(*)$, $0.02\,(\cdot)$, $0.01\,(-)$, $0.005\,(-\cdot)$

## 2.4 Numerical tests of the scheme

In the absence of boundaries, a von Neumann analysis shows that the time step restriction for our scheme is

$$\delta_t < \frac{h}{\sqrt{\frac{4\mu+\lambda}{\rho}}} = \frac{h}{\sqrt{c_p^2 + 2c_s^2}},$$

evaluated at all grid points and the minimum value taken. Although we have not performed a detailed spectral analysis for the scheme including boundary conditions, numerical tests have not indicated any additional restrictions on the time step due to the presence of stress free or non-reflecting boundaries.

In order to test the implementation of our method we first ran a number of computations with decreasing grid size $h$ and computed the discrete energy $C_e(t_n)$ at every time step. We started the computations with a non-zero displacement field and let it evolve with zero forcing, so $C_e(t_n)$ should remain constant. One boundary of the grid had a free surface condition and at all other boundaries we enforced zero displacements. The results are displayed in Figure 1.

As a second test we have checked the order of accuracy of the scheme using the *method of analytical solutions* (also known as *twilight-zone forcing* [6]). We modified the forcing functions $\mathbf{f}$ and $\mathbf{g}$ so that the solution of our test problem became a known function $\mathbf{u}^{\text{true}}(\mathbf{x}, t)$. We then solved the problem using our implementation of the method and compared our numerical results to the known solution on a succession of finer grids in order to check the convergence properties. Our constructed solution was

$$\begin{aligned} u^{\text{true}}(\mathbf{x}, t) &= \sin(\omega(x - ct)) \sin(\omega y) \sin(\omega z), \\ v^{\text{true}}(\mathbf{x}, t) &= \sin(\omega x) \sin(\omega(y - ct)) \sin(\omega z), \\ w^{\text{true}}(\mathbf{x}, t) &= \sin(\omega x) \sin(\omega y) \sin(\omega(z - ct)), \end{aligned}$$

| | $t = 1$ | |
|---|---|---|
| $h$ | $\|\|\mathbf{v}_h - \mathbf{u}^{\text{true}}\|\|_\infty$ | rate |
| 0.04 | 0.04331 | |
| 0.02 | 0.01062 | 4.079 |
| 0.01 | 0.002654 | 4.00 |
| 0.005 | 0.0006627 | 4.00 |

Table 1: Errors in max-norm for decreasing $h$ and smooth analytical solution $\mathbf{u}^{\text{true}}$. Convergence rate indicates second order convergence. Here $c = 1$ and $\omega = 2\pi$.

where $\omega$ and $c$ are constants. The material properties were chosen to vary smoothly according to

$$\mu(\mathbf{x}) = 1 + \cos^2(\pi x)\cos^2(\pi y)\cos^2(\pi z)$$
$$\lambda(\mathbf{x}) = 1 + \sin^2(\pi x)\sin^2(\pi y)\sin^2(\pi z)$$
$$\rho(\mathbf{x}) = 1.$$

As earlier a number of tests with increasingly fine grid spacing were run and the errors computed in the discrete max-norm. The discrete max-norm of a vector grid function $\mathbf{v}_h = (u_h, v_h, w_h)$ is defined as $||\mathbf{v}_h||_\infty = \max(\max_{i,j,k}|u_h|, \max_{i,j,k}|v_h|, \max_{i,j,k}|w_h|)$. Table 1 shows the results. As expected we get second order convergence when both the forcing and the solution are smooth. Non-smooth forcing and solutions are discussed in Section 4.

# 3 Truncating the computational domain

Since we are often interested in computing in open or half-open spaces were the physical boundaries are too far off to be included in the computational domain we need to truncate it by introducing artificial boundaries.

At the artificial boundaries of the domain, non-reflecting boundary conditions are imposed. There exist many different types of non-reflecting boundary conditions of different degrees of efficiency. No numerical non-reflecting boundary condition is perfect in that there will always be a certain amount of back scatter. The quality of the boundary condition is measured by the size of the reflected waves. These represent errors that propagate from the artificial boundary back into the computational domain.

We use non-reflecting boundary conditions of Clayton-Engquist type [7], where the idea is to impose a differential equation on the boundary. This boundary operator allows wave propagation only in the outward direction, and is an approximation of the elastic wave equation. A hierarchy of boundary conditions is obtained by successively increasing the order of the approximation. The first order non-reflecting boundary conditions for the boundaries $x = const$ are

$$u_t = \pm c_p u_x,\ v_t = \pm c_s v_x,\ w_t = \pm c_s w_x,$$

where the positive signs are taken for the lower boundary $x = 0$ and the negative signs for the upper boundary $x = a$. These are advection equations propagating waves out of domain, in the direction normal to the boundary. In the $y$- and $z$-directions, the conditions are similar advection equations in the direction normal to the boundary.

At the edges of the domain, we use compatibility conditions. For example, on the boundaries $x = 0$ and $y = 0$, the two conditions

$$u_t = c_p u_x,\ v_t = c_s v_x,\ w_t = c_s w_x, \quad x = 0,\ 0 \le y \le b,\ 0 \le z \le c,\ t \ge 0,$$

and

$$u_t = c_s u_y,\ v_t = c_p v_y,\ w_t = c_s w_y, \quad y = 0,\ 0 \le x \le a,\ 0 \le z \le c,\ t \ge 0,$$

hold. Equating the time derivatives along the edge gives

$$c_p u_x = c_s u_y, \tag{41}$$

$$c_s v_x = c_p v_y, \quad y = 0,\ x = 0,\ 0 \le z \le c,\ t \ge 0, \tag{42}$$

$$c_s w_x = c_s w_y, \tag{43}$$

This edge approximation is different from [7], where the first order conditions are applied in the diagonal direction at the edges. Our compatibility conditions are easier to implement, and have turned out in practice to have better stability properties.

Higher order non-reflecting conditions are more complicated, and their stability and well-posedness needs to be studied in detail in order to make them practically useful. We plan to present results on higher order non-reflecting boundary conditions in a future paper.

### 3.1 Discretization

The non-reflecting boundary conditions are discretized to second order accuracy by the box scheme at the boundary. For example, at the $x = 0$ boundary we have

$$\frac{u^{n+1}_{1,j,k} - u^n_{1,j,k} + u^{n+1}_{2,j,k} - u^n_{2,j,k}}{2\delta t} = (c_p)_{3/2,j,k} \frac{u^{n+1}_{2,j,k} - u^{n+1}_{1,j,k} + u^n_{2,j,k} - u^n_{1,j,k}}{2h}.$$

for $1 \le j \le N_y,\ 1 \le k \le N_z$. The equations for the displacements $v$ and $w$ are discretized analogously. For (41), we use the second order discretization

$$(c_p)_{3/2,3/2,k}(u_{2,1,k} - u_{1,1,k} + u_{2,2,k} - u_{1,2,k}) = (c_s)_{3/2,3/2,k}(u_{1,2,k} - u_{1,1,k} + u_{2,2,k} - u_{2,1,k})$$

around the edge points $(3/2, 3/2, k)$ to obtain

$$u_{1,1,k} = u_{2,2,k} + \frac{c_p + c_s}{c_p - c_s}(u_{2,1,k} - u_{1,2,k}) \quad 1 \le k \le N_z,$$

where $c_p$ and $c_s$ are evaluated at $(3/2, 3/2, k)$. Equation (42) is discretized similarly. The $w$-component along the edge can not be determined in this way, but it is not needed because there is no $xy$-derivative of $w$ in the elastic wave equation. The other edges are discretized analogously.

## 4 Singular source terms

Certain applications in elastic wave theory have source terms confined to small regions of space. For seismic applications these might represent fault slips or explosions. Since the grid size typically is larger than the support of the source, it is customary to approximate the separate sources at points in space, so that $\mathbf{f} = \sum_r \mathbf{f}^r$ and

$$\mathbf{f}^r = \delta(\mathbf{x} - \mathbf{x}_r) g^r(t) \mathbf{a}^r, \tag{44}$$

where $\delta(\mathbf{x})$ is Dirac's delta distribution, $g^r(t)$ describes the time dependence of the source, and $\mathbf{a}^r$ is a constant vector giving the direction of the force. These point forces can for instance be used to model

volcanic eruptions, or outside disturbances applied at the surface. However, to model realistic fault slips as point sources it is necessary to use force couples [3]. These are also called generalized body forces and are expressed as

$$\mathbf{f}^r = \nabla \cdot \delta(\mathbf{x} - \mathbf{x}_r)\mathfrak{M}^r g^r(t), \tag{45}$$

where $\mathfrak{M}^r(t)$ is a symmetric tensor called the source moment tensor with components $m_{xx}$, $m_{xy}$, etc.

Sources in the form of (44) and (45) with singular behavior in space requires a high degree of smoothness in time in order to avoid spatially non-smooth solutions. As we will show, smoothness and compact support in time will translate into smoothness in space.

## 4.1 Numerical modeling

For the point forces described by (44) the spatial dependence is of the general form $\delta(x)\delta(y)\delta(z)$ and for force couples (45) that expression will be differentiated in one direction, e.g. $\delta'(x)\delta(y)\delta(z)$. The solution of the continuous problems will become singular at the points where the forcing is applied and we cannot expect full convergence of the numerical solutions in any of the standard $L^p$ norms. However, by carefully approximating the Dirac delta distribution by a smooth regularized function on the grid it is possible to regain full point wise convergence away from the sources. Following [23, 21], we have used a hat function approximation for the Dirac distribution when approximating (44)

$$\delta^{\text{hat}}(x) = \frac{1}{h}\begin{cases} 1 - |x|/h, & |x| < h \\ 0, & \text{elsewhere,} \end{cases} \tag{46}$$

and a cubic polynomial for sources of type (45), where we need a derivative of the Dirac distribution

$$\delta^{\text{cube}}(x) = \frac{1}{h}\begin{cases} 1 - |x/h|/2 - |x/h|^2 + |x/h|^3/2, & |x| < h \\ 1 - 11|x/h|/6 + |x/h|^2 - |x/h|^3/6, & h < |x| < 2h \\ 0, & \text{elsewhere.} \end{cases} \tag{47}$$

The three dimensional functions are constructed as products of three one dimensional Dirac distribution approximations. The sources will thus end up distributed over a number of grid points.

In order to verify the implementations of the different body force types we have performed a number of tests comparing the numerical results to analytical solutions. For seismic applications the time dependence $g(t)$ typically has the form of a integrated Gaussian pulse or Ricker wavelet. These functions are $C^\infty$ but do not have compact support and the solution will remain singular at the forcing point for all times. For the numerical tests in this paper we have used high order polynomials with compact support which give solutions which are smooth after the initial transient and also simplify the analysis.

Even though the source terms are singular in space, smoothness in time will translate into smoothness in space away from the source. In order to demonstrate this we will look at the related problem of the scalar wave equation with singular spatial forcing. We study the problem on the unit cube with the forcing term applied at the center point $(0,0,0)$, zero initial data, and 1-periodic solution in all directions. In other words we want to solve

$$\begin{aligned} p_{tt} &= \nabla^2 p + \delta(x)\delta(y)\delta(z)g(t) \quad \mathbf{x} \in [-1/2 \quad 1/2]^3, \quad t \geq 0, \\ p(\mathbf{x}, t=0) &= p_t(\mathbf{x}, t=0) = 0, \\ p(\mathbf{x}, t) &= p(x+l, y+m, z+n, t), \quad (l,m,n) \in \mathbb{Z}. \end{aligned}$$

Here $g(t)$ is smooth and has compact support, i.e. $g(t) \equiv 0$ for $t \geq T$. We introduce a uniform grid with spacing $h = 1/(N+1)$, where $N$ is even, and discretize in space. We use the $\delta^{\text{hat}}$ function to approximate

the delta distribution. We define the three-dimensional discrete Fourier transform of a grid function as

$$f(\mathbf{x}) = \sum_{k_z,k_y,k_x} \hat{f}(k_x,k_y,k_z)e^{<\boldsymbol{\kappa},\mathbf{x}>},\ \hat{f}(k_x,k_y,k_z) = \sum_{k,j,i} \frac{f(\mathbf{x}_{i,j,k})}{(N+1)^3} e^{-<\boldsymbol{\kappa},\mathbf{x}_{i,j,k}>},$$

where $\mathbf{x}_{i,j,k} = (i-1/2, j-1/2, k-1/2)/(N+1)$, $\boldsymbol{\kappa} = 2\pi\imath(k_x,k_y,k_z)$, $<\cdot,\cdot>$ is the dot product, and all sums are from $-N/2$ to $N/2$. By Fourier transforming the discretized equations we get for the transformed variable $\hat{p} = \hat{p}(k_x,k_y,k_z,t)$,

$$\frac{d^2\hat{p}}{dt^2} = -\hat{\kappa}^2\hat{p} + \hat{\delta}g(t) \quad (k_x,k_y,k_z) \in [-N/2 \quad N/2], \tag{48}$$

where $\hat{\delta} = \hat{\delta}(k_x,k_y,k_z)$ is the transform of the discretized Dirac distributions

$$\hat{\delta}(k_x,k_y,k_z) = \sum_{k,j,i=0}^{1} \frac{e^{-<\boldsymbol{\kappa},\mathbf{x}_{i,j,k}>}}{8(N+1)^6},$$

and $\hat{\kappa} = \sqrt{4(N+1)^2(\sin^2(\frac{\pi k_x}{N+1}) + \sin^2(\frac{\pi k_y}{N+1}) + \sin^2(\frac{\pi k_z}{N+1}))}$. Equation (48) is solved by

$$\hat{p}(k_x,k_y,k_z,t) = \frac{\hat{\delta}}{\hat{\kappa}}\left[\sin(\hat{\kappa}t)\int_0^t \cos(\hat{\kappa}\tau)g(\tau)\,d\tau - \cos(\hat{\kappa}t)\int_0^t \sin(\hat{\kappa}\tau)g(\tau)\,d\tau\right]. \tag{49}$$

Integrating (49) by parts gives

$$\hat{p}(k_x,k_y,k_z,t) = \frac{\hat{\delta}}{\hat{\kappa}^2}\left[\sin^2(\hat{\kappa}t)g(t) - \sin(\hat{\kappa}t)\int_0^t \sin(\hat{\kappa}\tau)g'(\tau)d\tau + \cos^2(\hat{\kappa}t)g(t) - \cos(\hat{\kappa}t)\int_0^t \cos(\hat{\kappa}\tau)g'(\tau)d\tau\right].$$

Since $g(t) = 0$ for $t \geq T$ this reduces to

$$\hat{p}(k_x,k_y,k_z,t) = \frac{\hat{\delta}}{\hat{\kappa}^2}\left[-\sin(\hat{\kappa}t)\int_0^t \sin(\hat{\kappa}\tau)g'(\tau)\,d\tau - \cos(\hat{\kappa}t)\int_0^t \cos(\hat{\kappa}\tau)g'(\tau)\,d\tau\right], \quad t \geq T.$$

This procedure can be repeated as long as $g(t)$ can be differentiated and we will gain one order of $\hat{\kappa}$ each time, showing that the solution in real space $p(\mathbf{x},t)$ will be smooth for $t > T$ as long as $g(t)$ is sufficiently differentiable. If $g(t)$ does not tend to zero for large $t$ the solution will remain singular at the forcing point but will be smooth away from it.

## 4.2 Free space solutions

The free space Green's (dyadic) function $\mathfrak{G}(\mathbf{x},\mathbf{x}',t,t')$ , assuming a homogeneous material, is easily found in the literature [3]. Due to the trivial spatial dependence of the point forces the convolution reduces to a integral over $t'$. Furthermore for polynomial $g(t)$ the integration can be done analytically and a closed form solution obtained.

For the generalized body forces that contain spatial derivatives of the Dirac delta distribution the solution is obtained from the convolution of the source with the gradient of the Green's function. For our case where the source terms are point forces this simplifies to

$$\mathbf{u}(\mathbf{x},t) = \sum_r \int_{-\infty}^{t} \mathfrak{M}^r(t') : \nabla'\mathfrak{G}(\mathbf{x}-\mathbf{x}_r,\mathbf{x}',t,t')\,dt',$$

where the primed gradient operates on $\mathbf{x}'$.

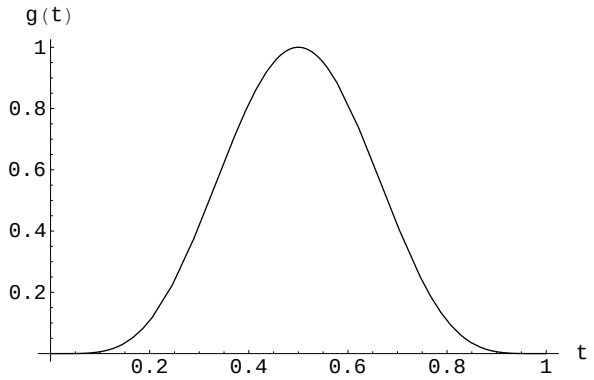


Figure 2: The behavior of the source strength over time. $g(t)$ has compact support on $[0,1]$ and is four times differentiable.

To verify the implementation and also to see what order of solution convergence can be expected for problems with singular sources, we have run a number of tests with point sources of the type given by (44) and (45). The solutions for the continuous case exhibits point singularities proportional to $1/|\mathbf{x}|$ for point forces (44) and $1/|\mathbf{x}|^2$ for point force couples (45), and it is interesting to see how the convergence of the numerical solutions were affected by the singularities.

The errors were measured in the discrete max-, 2− and 1-norms and computed at two different time levels. First during the transient phase when the solution is singular at the forcing point. Secondly, when the forcing has settled down to zero and the solution should be smooth everywhere. The 2− and 1−norms for a vector grid function $\mathbf{v}_h$ are defined as $||\mathbf{v}_h||_2 = h^3 \sum_{i,j,k}(|u_h|^2 + |v_h|^2 + |w_h|^2)$ and $||\mathbf{v}_h||_1 = h^3 \sum_{i,j,k}(|u_h| + |v_h| + |w_h|)$. Results are given in Table 2 and 3 for runs with four different grid sizes $h$. The behavior of $g(t)$ is shown in Figure 2.

As expected we do not achieve full convergence during the transient phase due to the singular behavior of the analytical solution. Furthermore, the convergence rate is lower the more singular the solution is. However, looking at the error away from the singularity we see that the error is smooth in space and decreases with the expected second order convergence, see Figure 3. For the case of a point moment source it is important to use the cubic regularized approximation of the Dirac distribution (47), otherwise the convergence order will be lower than two even away from the source.

After the initial transient the solution becomes smooth everywhere as expected and our results show convergence according to theory, see Tables 2 and 3.

## 4.3 Half spaces and Lamb's problem

Point forcing on the boundary of a half space is referred to as Lamb's problem [17]. Solutions for the two and three-dimensional cases have been presented by a number of authors with different degrees of applicability. For the case of a force applied normal to the surface $z = 0$, the general solution can be found in [19] and [8]. Similarly to the free space case we have tested the convergence at two different times with results given in Table 4. However, here we have only evaluated the error on the boundary as the analytical solution is not as easily obtained in the rest of the domain.

| | $t = 0.5$ | | | | | |
|---|---|---|---|---|---|---|
| $h$ | $\frac{\|\|\mathbf{v}_h-\mathbf{u}\|\|_\infty}{\|\|\mathbf{v}_h\|\|_\infty}$ | $\frac{\|\|\mathbf{v}_h-\mathbf{u}\|\|_2}{\|\|\mathbf{v}_h\|\|_2}$ | $\frac{\|\|\mathbf{v}_h-\mathbf{u}\|\|_1}{\|\|\mathbf{v}_h\|\|_1}$ | rate$^\infty$ | rate$^2$ | rate$^1$ |
| 0.04 | 0.04833 | 0.08293 | 0.1011 | | | |
| 0.02 | 0.04108 | 0.05174 | 0.03248 | 1.176 | 1.602 | 3.113 |
| 0.01 | 0.03936 | 0.03525 | 0.009970 | 1.043 | 1.467 | 3.257 |
| 0.005 | 0.03894 | 0.02470 | 0.002955 | 1.010 | 1.427 | 3.373 |
| | $t = 1.2$ | | | | | |
| $h$ | $\frac{\|\|\mathbf{v}_h-\mathbf{u}\|\|_\infty}{\|\|\mathbf{v}_h\|\|_\infty}$ | $\frac{\|\|\mathbf{v}_h-\mathbf{u}\|\|_2}{\|\|\mathbf{v}_h\|\|_2}$ | $\frac{\|\|\mathbf{v}_h-\mathbf{u}\|\|_1}{\|\|\mathbf{v}_h\|\|_1}$ | rate$^\infty$ | rate$^2$ | rate$^1$ |
| 0.04 | 0.04516 | 0.03984 | 0.04122 | | | |
| 0.02 | 0.01180 | 0.01001 | 0.01025 | 3.831 | 3.984 | 4.021 |
| 0.01 | 0.003023 | 0.002512 | 0.002560 | 3.907 | 3.988 | 4.004 |
| 0.005 | 0.0007592 | 0.0006287 | 0.0006400 | 3.983 | 4.000 | 4.00 |

Table 2: Relative error in $\mathbf{u}$ for the numerical solution of the free space problem with point forces at two different times in max-, $2-$ and $1-$norms.

| | $t = 0.5$ | | | | | |
|---|---|---|---|---|---|---|
| $h$ | $\frac{\|\|\mathbf{v}_h-\mathbf{u}\|\|_\infty}{\|\|\mathbf{v}_h\|\|_\infty}$ | $\frac{\|\|\mathbf{v}_h-\mathbf{u}\|\|_2}{\|\|\mathbf{v}_h\|\|_2}$ | $\frac{\|\|\mathbf{v}_h-\mathbf{u}\|\|_1}{\|\|\mathbf{v}_h\|\|_1}$ | rate$^\infty$ | rate$^2$ | rate$^1$ |
| 0.04 | 0.3051 | 0.2805 | 0.2272 | | | |
| 0.02 | 0.3208 | 0.2760 | 0.1154 | 0.9509 | 1.016 | 1.969 |
| 0.01 | 0.3253 | 0.2769 | 0.05759 | 0.9871 | 0.9967 | 2.003 |
| 0.005 | 0.3264 | 0.2782 | 0.02872 | 0.9970 | 0.9953 | 2.005 |
| | $t = 1.2$ | | | | | |
| $h$ | $\frac{\|\|\mathbf{v}_h-\mathbf{u}\|\|_\infty}{\|\|\mathbf{v}_h\|\|_\infty}$ | $\frac{\|\|\mathbf{v}_h-\mathbf{u}\|\|_2}{\|\|\mathbf{v}_h\|\|_2}$ | $\frac{\|\|\mathbf{v}_h-\mathbf{u}\|\|_1}{\|\|\mathbf{v}_h\|\|_1}$ | rate$^\infty$ | rate$^2$ | rate$^1$ |
| 0.04 | 0.1170 | 0.1016 | 0.09981 | | | |
| 0.02 | 0.03400 | 0.02762 | 0.02681 | 3.440 | 3.678 | 3.724 |
| 0.01 | 0.008872 | 0.007109 | 0.006855 | 3.833 | 3.885 | 3.908 |
| 0.005 | 0.002244 | 0.001793 | 0.001724 | 3.961 | 3.972 | 3.985 |

Table 3: Relative error in $\mathbf{u}$ for the numerical solution of the free space problem with point force couples at two different times in max-, $2-$ and $1-$norms.

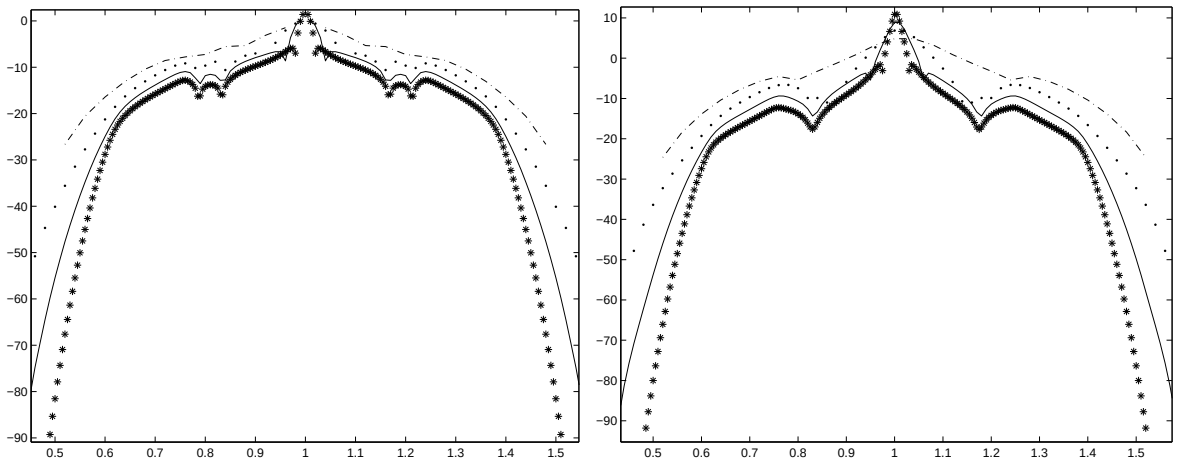

Figure 3: The 2−logarithm of the error along a line going through the source point for a point force (left) and a point moment source (right), both located at $x = 1$. The solution converges smoothly away from the source. $h = 0.04\,(-\cdot)$, $0.02\,(\cdot)$, $0.01\,(-)$, $0.005\,(*)$

| | $t = 0.5$ | | | | | |
|---|---|---|---|---|---|---|
| $h$ | $\frac{\|\|\mathbf{v}_h-\mathbf{u}\|\|_\infty}{\|\|\mathbf{v}_h\|\|_\infty}$ | $\frac{\|\|\mathbf{v}_h-\mathbf{u}\|\|_2}{\|\|\mathbf{v}_h\|\|_2}$ | $\frac{\|\|\mathbf{v}_h-\mathbf{u}\|\|_1}{\|\|\mathbf{v}_h\|\|_1}$ | rate$^\infty$ | rate$^2$ | rate$^1$ |
| 0.04 | 0.02797 | 0.08631 | 0.2007 | | | |
| 0.02 | 0.01758 | 0.05312 | 0.1102 | 1.591 | 1.625 | 1.821 |
| 0.01 | 0.01547 | 0.04002 | 0.05028 | 1.136 | 1.327 | 2.192 |
| 0.005 | 0.01696 | 0.03696 | 0.02305 | 0.9121 | 1.083 | 2.181 |
| | $t = 1.1$ | | | | | |
| $h$ | $\frac{\|\|\mathbf{v}_h-\mathbf{u}\|\|_\infty}{\|\|\mathbf{v}_h\|\|_\infty}$ | $\frac{\|\|\mathbf{v}_h-\mathbf{u}\|\|_2}{\|\|\mathbf{v}_h\|\|_2}$ | $\frac{\|\|\mathbf{v}_h-\mathbf{u}\|\|_1}{\|\|\mathbf{v}_h\|\|_1}$ | rate$^\infty$ | rate$^2$ | rate$^1$ |
| 0.04 | 0.2892 | 0.3081 | 0.3686 | | | |
| 0.02 | 0.1082 | 0.1186 | 0.1408 | 2.673 | 2.598 | 2.618 |
| 0.01 | 0.03138 | 0.03496 | 0.04175 | 3.448 | 3.392 | 3.372 |
| 0.005 | 0.008189 | 0.009194 | 0.01100 | 3.832 | 3.802 | 3.795 |

Table 4: Relative error in $\mathbf{u}$ for the numerical solution of Lamb's problem at two different times in max-, 2− and 1− norms.

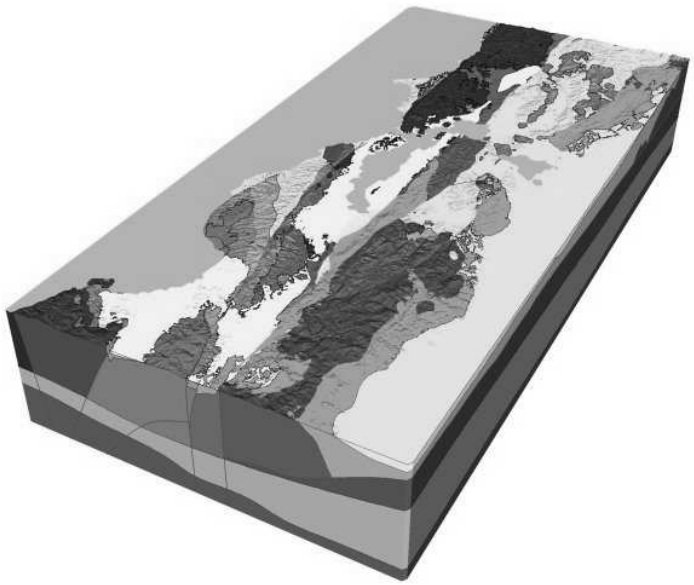

Figure 4: 3D perspective view of the USGS geologic model of the San Francisco bay area. Different shades of gray corresponds to different rock types.

# 5 Real world applications

Our finite difference method has been implemented in a code intended for general elastic wave propagation problems, but has so far mainly been used for seismic applications. The code has been written in C++ with occasional calls to Fortran routines for the computational kernels. Parallelization has been carried out using the C++ bindings to the MPI-2 libraries and we have observed good scalability for up to 1024 processors.

The code has been used for modeling a number of seismic events, and has been extensively compared to other existing codes and analytical approximations. The rest of this section will be devoted to a short example.

## 5.1 Earthquake modeling in the San Francisco bay area

The San Francisco bay area is a densely populated area that also has a high rate of seismic activity. Consequently there is a huge interest in trying to predict potential damage occurring due to earthquakes. As a step in this direction we have started doing earthquake simulations of local events where there is measurements available for comparison. As part of the earthquake hazards program at USGS, they have compiled a database containing detailed geological data for the bay area region together with an interface suitable for high performance computing [5]. Figure 4 shows a cut through the three-dimensional data illustrating the different rock types having different wave propagation properties.

As an example, we have simulated an earthquake from 1999/08/18, having an epicenter near Bolinas, California. Seismographic traces from the real event are available from multiple stations. We have compared our data to measurements from a broadband seismic station (Black Diamond Mine, near Antioch, California) at a distance of 72 km. A single point moment source 8 km below the surface was

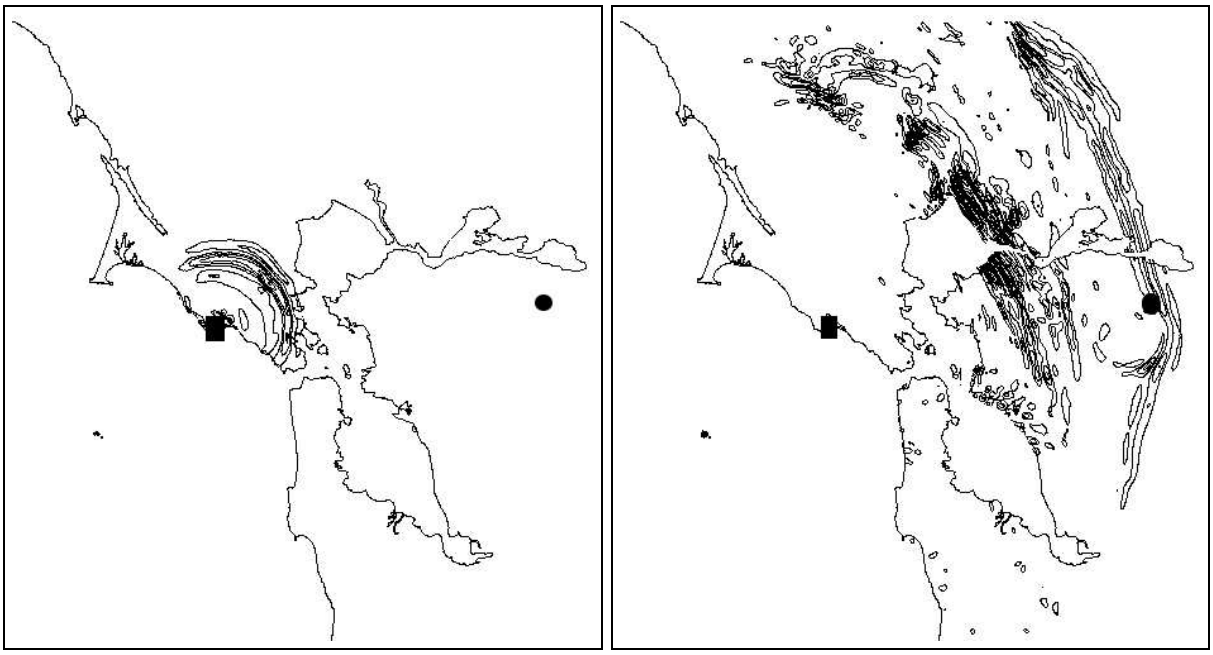

Figure 5: The computed solution on the surface 6.17 s (left), and 23.6 s (right) after the seismic event. The plots show contour lines of $|\nabla \times \mathbf{u}_t|$, illustrating the propagation of the transverse waves. The epicenter of the event is located at the ■ and the seismic station is located at the •.

used to model the seismic event, and the grid size was 0.2 km. An added complication here was that the domain contained large areas of shallow water where the material properties are difficult to average correctly. Figure 5 shows snapshots of the solution at two different times on the surface while Figure 6 shows the measured displacement data as compared to our computation at the seismic station.

The results in Figure 6 corresponds reasonably well to measurements, lending credibility to both the geological model and the modeling of the seismic source. Further validation of the bay area model will be reported elsewhere.

# 6 Conclusions

The finite difference method described in this paper has been shown to work well not only for simple test problems but also for real world applications with highly irregular data. Here we give a brief glimpse of some work in progress and future plans for extensions of the method.

When the computational domain includes acoustic materials such as water, the method needs to be modified in order to get good results. For water, $\mu = 0$ and only longitudinal waves can propagate, making the theory of Section 2 incomplete. We have started working on the mixed elastic-acoustic case and initial results look promising.

As mentioned in the beginning we plan to include and also to extend the application areas to more general engineering problems. Geometrical features will be handled by using embedded boundaries intersecting the Cartesian grid. Discretizing the stress free boundary condition efficiently on the embedded boundaries is an ongoing research topic. We also want to use a similar technique to accurately handle internal boundaries between different materials and to satisfy the correct jump conditions on the internal boundary instead of applying the finite difference stencil across them. Work in this direction is reported

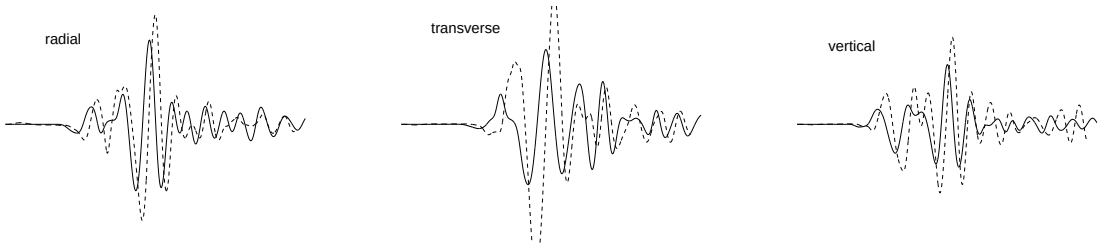


Figure 6: Recorded and computed ground motion at the Black Diamond Mine over a time interval of 80 s. The motion has been decomposed into components in a cylindrical coordinate system having its origin at the epicenter of the event, near Bolinas. Solid lines represent the simulation results, and dashed lines the measurements. Both the measured and the computed signals have been bandpass filtered to include frequencies between 0.02-0.2 Hz.

in [14].

We also want to look closer at non-reflecting boundary conditions. In seismic computations, there are significant uncertainties in material data and in the source terms. For this reason, we believe the non-reflecting boundary conditions can be fairly simple. We only assume that the error from the artificial boundary does not dominate other errors in the computed solution. In the future we would like to quantify this and also examine more advanced conditions and see if they make a difference for real world applications.

## Acknowledgments

The authors would like to thank Artie Rodgers for a lot of helpful advice on seismology and related subjects, Steve Blair and Hrvoje Tkalcic for the extensive testing of the code and visualization work they have carried out, and finally Kathleen McCandless who has been the main architect of the new parallel code.

## A Self-adjointness of the spatial operator (Lemma 1)

It is straight forward to show the following summation by parts identities:

$$(w, D_-^z v)_h = -(D_+^z w, v)_h - \frac{h^2}{2}\sum_{i,j}\left(w_{i,j,2}v_{i,j,1} + w_{i,j,1}v_{i,j,0}\right) + h^2\sum_{i,j} w_{i,j,N_z}v_{i,j,N_z-1}, \tag{50}$$

$$(w, \widetilde{D_0^z} v)_h = -(\widetilde{D_0^z} w, v)_h - h^2\sum_{i,j} w_{i,j,1}v_{i,j,1} + \frac{h^2}{2}\sum_{i,j}\left(w_{i,j,N_z-1}v_{i,j,N_z} + w_{i,j,N_z}v_{i,j,N_z-1}\right), \tag{51}$$

where $\sum_{i,j} = \sum_{i=1}^{N_x-1}\sum_{j=1}^{N_y-1}$. Since the solution satisfies periodic boundary conditions in the $x$ and $y$-directions, we have

$$(w, D_-^x v)_h = -(D_+^x w, v)_h, \quad (w, D_0^x v)_h = -(D_0^x w, v)_h, \tag{52}$$

$$(w, D_-^y v)_h = -(D_+^y w, v)_h, \quad (w, D_0^y v)_h = -(D_0^y w, v)_h. \tag{53}$$

Consider the three terms in the left hand side of (27): $LHS := I + II + III$,

$$I = \left(u^0, L^{(u)}(u^1, v^1, w^1)\right)_h, \quad II = \left(v^0, L^{(v)}(u^1, v^1, w^1)\right)_h, \quad III = \left(w^0, L^{(w)}(u^1, v^1, w^1)\right)_h.$$

Applying the summation by parts identities (50)-(53) on the first term gives

$$\begin{aligned} I = &- \left(D_+^x u^0, E_{1/2}^x(2\mu+\lambda) D_+^x u^1\right)_h - \left(D_+^y u^0, E_{1/2}^y(\mu) D_+^y u^1\right)_h - \left(D_+^z u^0, E_{1/2}^z(\mu) D_+^z u^1\right)_h \\ &- \left(D_0^x u^0, \lambda D_0^y v^1 + \lambda \widetilde{D_0^z} w^1\right)_h - \left(D_0^y u^0, \mu D_0^x v^1\right)_h - \left(\widetilde{D_0^z} u^0, \mu D_0^x w^1\right)_h + B^{(u)}, \end{aligned} \quad (54)$$

where the boundary terms are

$$\begin{aligned} B^{(u)} = &- \frac{h^2}{2} \sum_{i,j} \left(u^0_{i,j,2} \mu_{i,j,3/2} D_+^z u^1_{i,j,1} + u^0_{i,j,1} \mu_{i,j,1/2} D_+^z u^1_{i,j,0}\right) \\ &- h^2 \sum_{i,j} u^0_{i,j,1} \mu_{i,j,1} D_0^x w^1_{i,j,1} + h^2 \sum_{i,j} u^0_{i,j,N_z} \mu_{i,j,N_z-1/2} D_+^z u^1_{i,j,N_z-1} \\ &+ \frac{h^2}{2} \sum_{i,j} \left(u^0_{i,j,N_z-1} \mu_{i,j,N_z} D_0^x w^1_{i,j,N_z} + u^0_{i,j,N_z} \mu_{i,j,N_z-1} D_0^x w^1_{i,j,N_z-1}\right). \end{aligned}$$

The homogeneous Dirichlet boundary condition (24) gives

$$u^0_{i,j,N_z} = 0, \quad D_0^x w^1_{i,j,N_z} = 0.$$

Hence, the third and fourth terms in $B^{(u)}$ vanish. To analyze the first term, we note that

$$u^0_{i,j,2} = u^0_{i,j,1} + h D_+^z u^0_{i,j,1}.$$

Therefore,

$$\begin{aligned} B^{(u)} = -\frac{h^2}{2} \sum_{i,j} u^0_{i,j,1} \left(\mu_{i,j,3/2} D_+^z u^1_{i,j,1} + \mu_{i,j,1/2} D_+^z u^1_{i,j,0} + 2\mu_{i,j,1} D_0^x w^1_{i,j,1}\right) \\ - \frac{h^3}{2} \sum_{i,j} \mu_{i,j,3/2} D_+^z u^0_{i,j,1} D_+^z u^1_{i,j,1}. \end{aligned} \quad (55)$$

The first term in (55) vanishes because of the free-surface boundary condition (21) and we arrive at

$$B^{(u)} = -\frac{h^3}{2} \sum_{i,j} \mu_{i,j,3/2} D_+^z u^0_{i,j,1} D_+^z u^1_{i,j,1}.$$

The second term in $LHS$ can be analyzed in the same way giving

$$\begin{aligned} II = &- \left(D_+^x v^0, E_{1/2}^x(\mu) D_+^x v^1\right)_h - \left(D_+^y v^0, E_{1/2}^y(2\mu+\lambda) D_+^y v^1\right)_h - \left(D_+^z v^0, E_{1/2}^z(\mu) D_+^z v^1\right)_h \\ &- \left(D_0^x v^0, \mu D_0^y u^1\right)_h - \left(D_0^y v^0, \lambda D_0^x u^1 + \lambda \widetilde{D_0^z} w^1\right)_h - \left(\widetilde{D_0^z} v^0, \mu D_0^y w^1\right)_h + B^{(v)}, \end{aligned} \quad (56)$$

where

$$B^{(v)} = -\frac{h^3}{2} \sum_{i,j} \mu_{i,j,3/2} D_+^z v^0_{i,j,1} D_+^z v^1_{i,j,1}.$$

For the third term in $LHS$ we get

$$III = -\left(D_+^x w^0, E_{1/2}^x(\mu) D_+^x w^1\right)_h - \left(D_+^y w^0, E_{1/2}^y(\mu) D_+^y w^1\right)_h - \left(D_+^z w^0, E_{1/2}^z(2\mu+\lambda) D_+^z w^1\right)_h$$
$$- \left(D_0^x w^0, \mu \widetilde{D}_0^z u^1\right)_h - \left(D_0^y w^0, \mu \widetilde{D}_0^z v^1\right)_h - \left(\widetilde{D}_0^z w^0, \lambda D_0^x u^1 + \lambda D_0^y v^1\right)_h + B^{(w)}, \quad (57)$$

where

$$B^{(w)} = -\frac{h^3}{2} \sum_{i,j} (2\mu_{i,j,3/2} + \lambda_{i,j,3/2}) D_+^z w_{i,j,1}^0 D_+^z w_{i,j,1}^1.$$

After applying the same summation by parts rules to the right hand side of (27) it is straight forward to verify that the right hand side equals the left hand side. □

# B Ellipticity of the spatial operator (Lemma 3)

We will mimic the construction of the energy in the continuous case by exploring the identity

$$D_-^x E_{1/2}^x(\mu) D_+^x u = D_0^x \left(\mu D_0^x u\right) - \frac{h^2}{4} D_+^x D_-^x \left(\mu D_+^x D_-^x u\right)$$

and the corresponding expressions in the $y$- and $z$-directions. We have

$$\widetilde{L}^{(u)}(u,v,w) =$$
$$D_-^x \left(E_{1/2}^x(2\mu+\lambda) D_+^x u\right) + D_-^y \left(E_{1/2}^y(\mu) D_+^y u\right) + D_-^z \left(E_{1/2}^z(\mu) D_+^z u\right)$$
$$+ D_0^x \left(\lambda D_0^y v + \lambda D_0^z w\right) + D_0^y \left(\mu D_0^x v\right) + D_0^z \left(\mu D_0^x w\right)$$
$$= 2 D_-^x \left(E_{1/2}^x(\mu) D_+^x u\right) + D_0^x \left(\lambda \left(D_0^x u + D_0^y v + D_0^z w\right)\right)$$
$$+ D_0^y \left(\mu \left(D_0^y u + D_0^x v\right)\right) + D_0^z \left(\mu \left(D_0^z u + D_0^x w\right)\right)$$
$$- \frac{h^2}{4} \left(D_+^x D_-^x (\lambda D_+^x D_-^x u) + D_+^y D_-^y (\mu D_+^y D_-^y u) + D_+^z D_-^z (\mu D_+^z D_-^z u)\right)$$

Summation by parts gives

$$\left(u, \widetilde{L}^{(u)}(u,v,w)\right)_2 =$$
$$- 2\left(D_+^x u, E_{1/2}^x(\mu) D_+^x u\right)_2 - \left(D_0^x u, \lambda \left(D_0^x u + D_0^y v + D_0^z w\right)\right)_2$$
$$- \left(D_0^y u, \mu \left(D_0^y u + D_0^x v\right)\right)_2 - \left(D_0^z u, \mu \left(D_0^z u + D_0^x w\right)\right)_2$$
$$- \frac{h^2}{4} \left(\left(D_+^x D_-^x u, \lambda D_+^x D_-^x u\right)_2 + \left(D_+^y D_-^y u, \mu D_+^y D_-^y u\right)_2 + \left(D_+^z D_-^z u, \mu D_+^z D_-^z u\right)_2\right)$$

The terms $\left(v, \widetilde{L}^{(v)}\right)$ and $\left(w, \widetilde{L}^{(w)}\right)$ can be analyzed in a similar manner. The resulting expression can be written as (33). □

# C Accuracy (Lemma 4)

We will prove the accuracy of the semi-discrete equations by showing that it is equivalent to another approximation which clearly is second order accurate. In particular, we want to analyze the accuracy of the

spatial discretization (18), (19), (20) at the $z = 0$ boundary, where the free surface boundary condition is applied. At this boundary, the operator $\widetilde{D_0^z}$ simplifies to $D_+^z$, which would appear to only give a first order accurate difference formula. However, we proceed to show that this difference formula, in combination with the discrete free-surface boundary condition, indeed results in a second order approximation.

We start by eliminating the ghost points above the free surface from the semi-discrete system (18), (19), (20), subject to the boundary conditions (21), (22), and (23). To save space, we only go through the details for (18) subject to (21). The terms in $L^{(u)}$ that contain $z$-differences on the $z = 0$ grid line are

$$T_{i,j} =: D_-^z \left(\mu_{i,j,3/2} D_+^z u_{i,j,1}\right) + D_0^x \left(\lambda_{i,j,1} D_+^z w_{i,j,1}\right) + D_+^z \left(\mu_{i,j,1} D_0^x w_{i,j,1}\right),$$

The free surface boundary condition (21) gives

$$\mu_{i,j,1/2} D_+^z u_{i,j,0} = -\mu_{i,j,3/2} D_+^z u_{i,j,1} - 2\mu_{i,j,1} D_0^x w_{i,j,1},$$

Hence,

$$T_{i,j} = \frac{2}{h}\left[\mu_{i,j,3/2} D_+^z u_{i,j,1} + \mu_{i,j,1} D_0^x w_{i,j,1}\right] + D_0^x \left(\lambda_{i,j,1} D_+^z w_{i,j,1}\right) + D_+^z \left(\mu_{i,j,1} D_0^x w_{i,j,1}\right). \tag{58}$$

We compare the spatial discretization to a fully centered scheme where the terms in $L^{(u)}$ that contain $z$-differences on the $z = 0$ grid line are

$$\widetilde{T}_{i,j} =: D_-^z \left(\mu_{i,j,3/2} D_+^z u_{i,j,1}\right) + D_0^x \left(\lambda_{i,j,1} D_0^z w_{i,j,1}\right) + D_0^z \left(\mu_{i,j,1} D_0^x w_{i,j,1}\right), \tag{59}$$

We can perturb the free surface boundary condition (21) by a second order term,

$$\frac{1}{2}\left(\mu_{i,j,3/2} D_+^z u_{i,j,1} + \mu_{i,j,1/2} D_+^z u_{i,j,0}\right) + \mu_{i,j,1} D_0^x w_{i,j,1} = h^2 R_{i,j}. \tag{60}$$

The resulting spatial discretization will be second order accurate as long as $R$ is a difference operator which is bounded independently of $h$ for smooth functions. We will determine $R$ such that (59) subject to (60) is equivalent to (58). The boundary condition (60) gives

$$\mu_{i,j,1/2} D_+^z u_{i,j,0} = -\mu_{i,j,3/2} D_+^z u_{i,j,1} - 2\mu_{i,j,1} D_0^x w_{i,j,1} + 2h^2 R_{i,j}. \tag{61}$$

Using (61), (59) can be written

$$\widetilde{T}_{i,j} = \frac{2}{h}\left[\mu_{i,j,3/2} D_+^z u_{i,j,1} + \mu_{i,j,1} D_0^x w_{i,j,1}\right] + D_0^x \left(\lambda_{i,j,1} D_0^z w_{i,j,1}\right) + D_0^z \left(\mu_{i,j,1} D_0^x w_{i,j,1}\right) + 2hR_{i,j}.$$

Hence, $T = \widetilde{T}$ if

$$D_0^x \left(\lambda_{i,j,1} D_+^z w_{i,j,1}\right) + D_+^z \left(\mu_{i,j,1} D_0^x w_{i,j,1}\right) = D_0^x \left(\lambda_{i,j,1} D_0^z w_{i,j,1}\right) + D_0^z \left(\mu_{i,j,1} D_0^x w_{i,j,1}\right) + 2hR_{i,j}.$$

We have

$$D_0^z w = D_+^z w - \frac{h}{2} D_+^z D_-^z w,$$

which gives

$$R_{i,j} = \frac{1}{4} D_0^x (\lambda_{i,j,1} D_+^z D_-^z w_{i,j,1}) + \frac{1}{4} D_+^z D_-^z \left(\mu_{i,j,1} D_0^x w_{i,j,1}\right).$$

Similar calculations show that the boundary conditions (22) and (23) can be perturbed by second order terms to account for the difference between a fully centered and a one-sided spatial discretization in $L^{(v)}$ and $L^{(w)}$, respectively.

This proves that the semi-discrete approximation (18)-(20) subject to the boundary conditions (21)-(23) is second order accurate. □

**Note:** Inserting the expression for $R_{i,j}$ into (60) shows that the fully centered approximation couples all ghost points ($k = 0$) along the free surface. Hence, using this formulation would require a linear system to be solved to obtain the ghost point values at each time step. As we have demonstrated, the same solution can be obtained without solving a linear system by using our one-sided formula on the boundary.

# References


[1] Z. S. Alterman and A. Rotenberg. Seismic waves in a quarter plane. *Bulletin of the Seismological Society of America*, 59, 1969.

[2] J. M. Ball. Some open problems in elasticity. In *Geometry, Mechanics, and Dynamics*. Springer Verlag, 2002.

[3] Ari Ben-Menahem and Sarva Jit Singh. *Seismic Waves and Sources*. Dover Publications, 2000.

[4] Sylvie Benzoni-Gavage, Frédéric Rousset, Denis Serre, and Kevin Zumbrun. Generic types and transitions in hyperbolic initial-boundary value problems. *Proceedings (A) of the Royal Soc. of Edinburgh*, 132A, 2002.

[5] Thomas M. Brocher. Compressional and shear wave velocity versus depth in the San Francisco bay area, California: Rules for USGS bay area velocity model 05.0.0. Technical report, USGS Open-File Report 2005-1317, 2005.

[6] G. Chesshire and W. Henshaw. Composite overlapping meshes for the solution of partial differential equations. *Journal of Computational Physics*, 90, 1990.

[7] Robert Clayton and Björn Engquist. Absorbing boundary conditions for acoustic and elastic wave equations. *Bulletin of the Seismological Society of America*, 67, 1977.

[8] A. Cemal Eringen and Erdoğan S. Şuhubi. *Elastodynamics, Volume II*. Elsevier, 1975.

[9] Takashi Furumura. Large-scale parallel simulation of seismic wave propagation and strong ground motions for the past and future earthquakes in Japan. *Journal of the Earth Simulator*, 3, 2005.

[10] A. Ilan and D. Loewenthal. Instability of finite difference schemes due to boundary conditions in elastic media. *Geophysical Prospecting*, 24, 1976.

[11] Almoga Ilan. Stability of finite difference schemes for the problem of elastic wave propagation in a quarter plane. *Journal of Computational Physics*, 29, 1978.

[12] Dimitri Komatitsch and Jeroen Tromp. Introduction to the spectral element method for three-dimensional seismic wave propagation. *Geophysical Journal International*, 139, 1999.

[13] Heinz-Otto Kreiss and N. Anders Petersson. A second order accurate embedded boundary method for the wave equation with dirichlet data. Technical report, UCRL-JRNL-202686, 2004. submitted to SIAM J. Sci. Comput.

[14] Heinz-Otto Kreiss and N. Anders Petersson. An embedded boundary method for the wave equation with discontinuous coefficients. Technical report, UCRL-JRNL-215702, 2005. submitted to SIAM J. Sci. Comput.

[15] Heinz-Otto Kreiss, N. Anders Petersson, and Jacob Yström. Difference approximations for the second order wave equation. *SIAM Journal on Numerical Analysis*, 40, 2002.

[16] Heinz-Otto Kreiss, N. Anders Petersson, and Jacob Ystrom. Difference approximations of the Neumann problem for the second order wave equation. *SIAM Journal on Numerical Analysis*, 42, 2004.

[17] Horace Lamb. On the propagation of tremors over the surface of an elastic solid. *Phil. Trans. Roy. Soc. London, Ser. A*, 203, 1904.

[18] R. Madariaga. Dynamics of an expanding circular fault. *Bulletin of the Seismological Society of America*, 66, 1976.

[19] Harold M. Mooney. Some numerical solutions for Lamb's problem. *Bulletin of the Seismological Society of America*, 64, 1974.

[20] Chaim L. Pekeris and Hanna Lifson. Motion of the surface of a uniform elastic half-space produced by a buried pulse. *The Journal of the Acoustical Society of America*, 29, 1957.

[21] Anna-Karin Tornberg and Björn Engquist. Numerical approximation of singular source terms in differential equations. *Journal of Computational Physics*, 200, 2004.

[22] John E. Vidale and Robert W. Clayton. A stable free-surface boundary condition for two-dimensional elastic finite-difference wave simulation. *Geophysics*, 51, 1986.

[23] Johan Waldén. On the approximation of singular source terms in differential equations. *Numerical Methods for Partial Differential Equations*, 15, 1999.